Kovove Mater. 63 2025 79–92
DOI: 10.31577/km.2025.2.79

Influence of gas-shielded welding process on the microstructure and properties of joints of 1100 MPa high-strength steel

Long Chen, Wei Li, Kun Liu, JiaSheng Zou*

College of Materials Science and Engineering, Jiangsu University of Science and Technology, Zhenjiang 212100, P. R. China

Received 11 December 2024, received in revised form 4 April 2025, accepted 8 April 2025

Abstract

Flux-cored wire CO_2 gas shielded welding of Q1100E high-strength steel was carried out for different inter-pass temperatures and bevel forms. This work investigated the effects of inter-pass temperature and bevel form on the microstructure and mechanical properties of welded joints. The results show that the microstructure of welding metal transforms from ferrite and granular bainite to lath martensite and granular bainite as the inter-pass temperature decreases, the heat-affected zone organization, the trend of coarsening of the lath martensite becomes smaller, and the number of granular bainite is relatively small. With the decrease of the bevel angle, the weld organization is still lath martensite + granular bainite, the lath martensite roughening degree decreases, and the number of granular bainite becomes smaller. Furthermore, as the inter-pass temperature decreases, the tensile strength of the joint increases and the impact toughness of the HAZ increases. As the bevel angle decreases, the tensile strength of the joint continues to grow and the impact toughness of the HAZ increases further. The maximum microhardness of the coarse grain zone was obtained when the inter-pass temperature was 30 ℃ and the bevel was 40 ℃V.

K e y w o r d s: Q1100E, CO_2 gas shielded welding, inter-pass temperature, beveling form

1. Introduction

High-strength steel is a lightweight steel with excellent plastic toughness [1, 2]. Welding is a key technology in manufacturing high-strength steel components, directly restricting or even determining the application of high-strength steel components, substantial components and service life [3–5]. With the increase in the strength of high-strength steel, the weldability of high-strength steel will be reduced, the difficulty of welding will be increased, the stability after welding will be reduced, the plastic toughness will be worse, and the crack sensitivity will increase [6, 7]. The defects, such as embrittlement and softening, will be easily produced in the heat-affected zone. Domestic and foreign studies have shown [8–12] that inter-pass temperature has an important effect on the welded parts of high-strength steel [13–15]. The inter-pass temperature affects the microstructure and property changes of high-strength steel because the shift in interlayer temperature causes a change in cooling time, affecting the microstructure and property changes of high-strength steel [16]. The design of the bevel form and control of inter-pass temperature are important factors affecting weld quality [17, 18].

Lan et al. [19] used three different heat input processes to study the microstructure evolution and the corresponding mechanical properties of the weldments, and based on the experimental results, the acceptable welding parameters of the studied steels were determined to obtain a good balance of high strength and toughness in welded joints. A comparative evaluation of the mechanical properties and microstructural characteristics of shielded metal arc (SMA), gas metal arc (GMA), and friction stir welded (FSW) joints of naval-grade, high-strength, low-alloy steel was conducted by Nathan et al. [20]. It was found that using the FSW process eliminated the problems associated with the fusion welding process and resulted in superior mechanical properties compared to GMA and

*Corresponding author: e-mail address: zjzoujs@just.edu.cn

Table 1. Chemical composition of base materials and wires (wt.%)

Materials	C	Mn	Si	Ni	Cr	Cu	Al	Nb	Mo	V	Ti
Q1100E	0.169	0.982	0.299	1.167	0.441	0.223	0.083	0.018	0.367	0.027	0.004
1100L-MC	0.086	1.57	0.624	2.432	0.554	0.069	0.032	0.012	0.423	0.24	0.015

Table 2. Mechanical properties of base materials and wires

Test material	$R_{p0.2}$ (MPa)	R_m (MPa)	Shock absorption (J) (–40 °C)
Q1100E	1188	1469	57, 56, 57
1100L-MC	1076	1130	39, 41, 38

SMA welded joints. Chen Sun et al. [21] used different austenitization temperatures to obtain medium carbon low alloy steels with different initial states and investigated the effects of these factors on the tempered carbides of MCLA steels and the impact toughness of MCLA steels. The results show that the austenitization temperature can effectively control the matrix carbon content and lath martensite substructure size, and the spheroidization of carbides is beneficial to improve the impact toughness.

Haslberger et al. [22] studied the martensitic all--weld metal sample with an approximate yield strength of 1000 MPa. The reduction in manganese and silicon content resulted in microstructure refinement and reduction in austenite grain size and effective grain size. Furthermore, a higher average grain boundary misorientation was measured, positively influencing the toughness. An addition of vanadium caused the formation of vanadium-rich clusters, which increased the strength of the all-weld metal significantly. Dong et al. [23] studied the microstructure and mechanical properties of the butt joint of 1100 MPa grade hot-rolled low-carbon steel by laser welding. The results show that the yield strength and tensile strength of the laser welded joint reached 100.2 and 99.5 % of the base material (BM), respectively. However, the elongation of the welded joint only reached about 60 % of BM. The minimum and maximum hardness values were obtained in the incomplete recrystallization zone. Liu et al. [24] studied the influence of heat input on the microstructure and mechanical properties of low-matched high-tensile steel welded joints. The results show that when the heat input is 11.9 kJ cm^{-1}, the tensile strength is 798.45 MPa and the ballistic work is 69 J. The weld metal microstructure is mainly composed of primary ferrite and acicular ferrite. The width of the dendrite and grain size of the weld metal microstructure increase when heat input is prolonged.

Domestic and international research on high--strength steels is limited to yield strength below 1000 MPa. However, this paper investigates high--strength steels with a yield strength of 1100 MPa. Secondly, research in China on high-strength steels focuses on testing conventional mechanical properties, neglecting studies on changes in microstructure during the welding process. In this work, 8 mm thick 1100 MPa level high-strength steel was used for the flux-cored wire gas-shielded welding for plate butt welding test. OM, SEM, EDS, and mechanical properties tests of welded joints were employed to study microstructure and mechanical properties. The effect of the inter-pass temperature and the bevel form was investigated on the microstructure and properties of 1100 MPa welded joints.

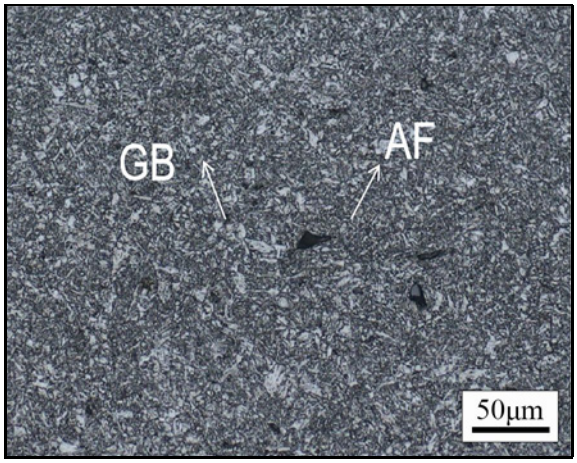

Fig. 1. Microstructure of Q1100E base metal.

2. Materials and methods

The base material selected for the test is a steel plate of Q1100E with a plate thickness of 8 mm. The microstructure of the Q1100E base material is shown in Fig. 1, which is mainly dominated by granular bainite and acicular ferrite. Burle 1100L-MC flux-cored wire was used for the welding process, with a wire diameter of 1.2 mm. The chemical composition of the test material is shown in Table 1, and the mechanical properties of the test material are shown in Table 2.

The 8 mm thick Q1100E was welded by flux-

Table 3. The parameters of the backing welding process

Welding current (A)	Welding voltage (V)	Welding speed (cm min^{-1})	Beveling form	Inter-pass temperature (°C)	Weld heat input (kJ cm^{-1})
110–160	14–19	15–18	60 °V	150	4.2–6.9
			60 °V	30	
			40 °V	30	

Table 4. The parameters of the cosmetic welding process

Welding current (A)	Welding voltage (V)	Welding speed (cm min^{-1})	Beveling form	Inter-pass temperature (°C)	Weld heat input (kJ cm^{-1})
230–240	23–25	35–40	60 °V	150	5.8–6.2
			60 °V	30	
			40 °V	30	

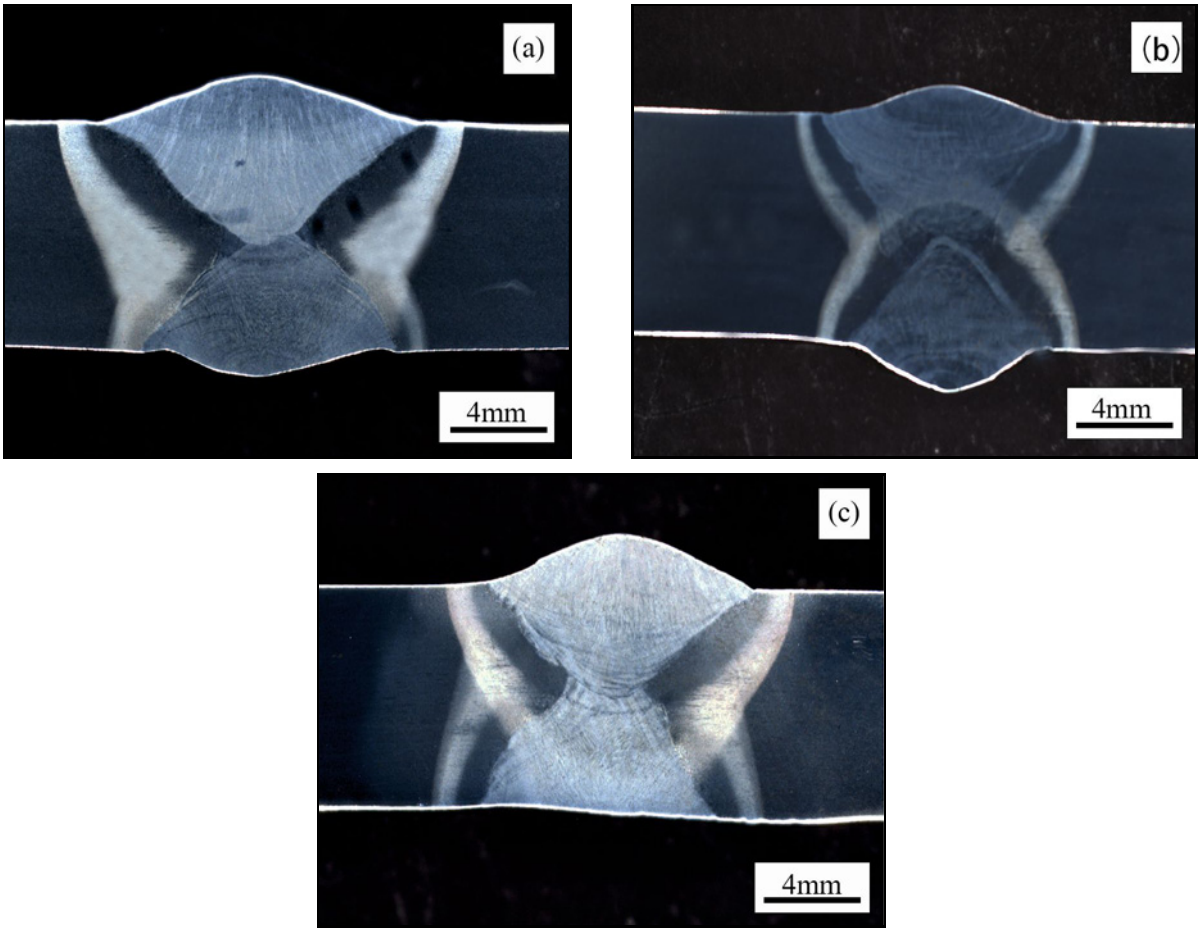

Fig. 2. Macro joints with different welding process parameters: (a) Inter-pass temperature 150 °C, 60 °V-bevel; (b) Inter-pass temperature 30 °C, 60 °V-bevel; and (c) Inter-pass temperature 30 °C, 40 °V-bevel.

cored gas shielded welding and Borel 1100L-MC powder-cored gas-shielded wire. The base materials are beveled at 40° and 60°. The specific welding parameters are shown in Tables 3 and 4. The specimens

were cooled to room temperature after welding.

The welded joints were cut through wire electrical discharge machining. The samples for metallographic analysis were ground with 100–2000# SiC grit paper and polished with the diamond abrasive paste. The metallographic corrosion was carried out with a formula of 4 ml HNO_3 + 96 ml C_2H_5OH.

An Axio Observer 3m Inverted microscope was used to observe the metallographic microstructure of the welded joints. The microstructure, elemental distribution, and fracture morphology were investigated through the field emission scanning electron microscope (ZEISS Merlin Compact) and the energy dispersive spectrometer (EDS). An electronic universal

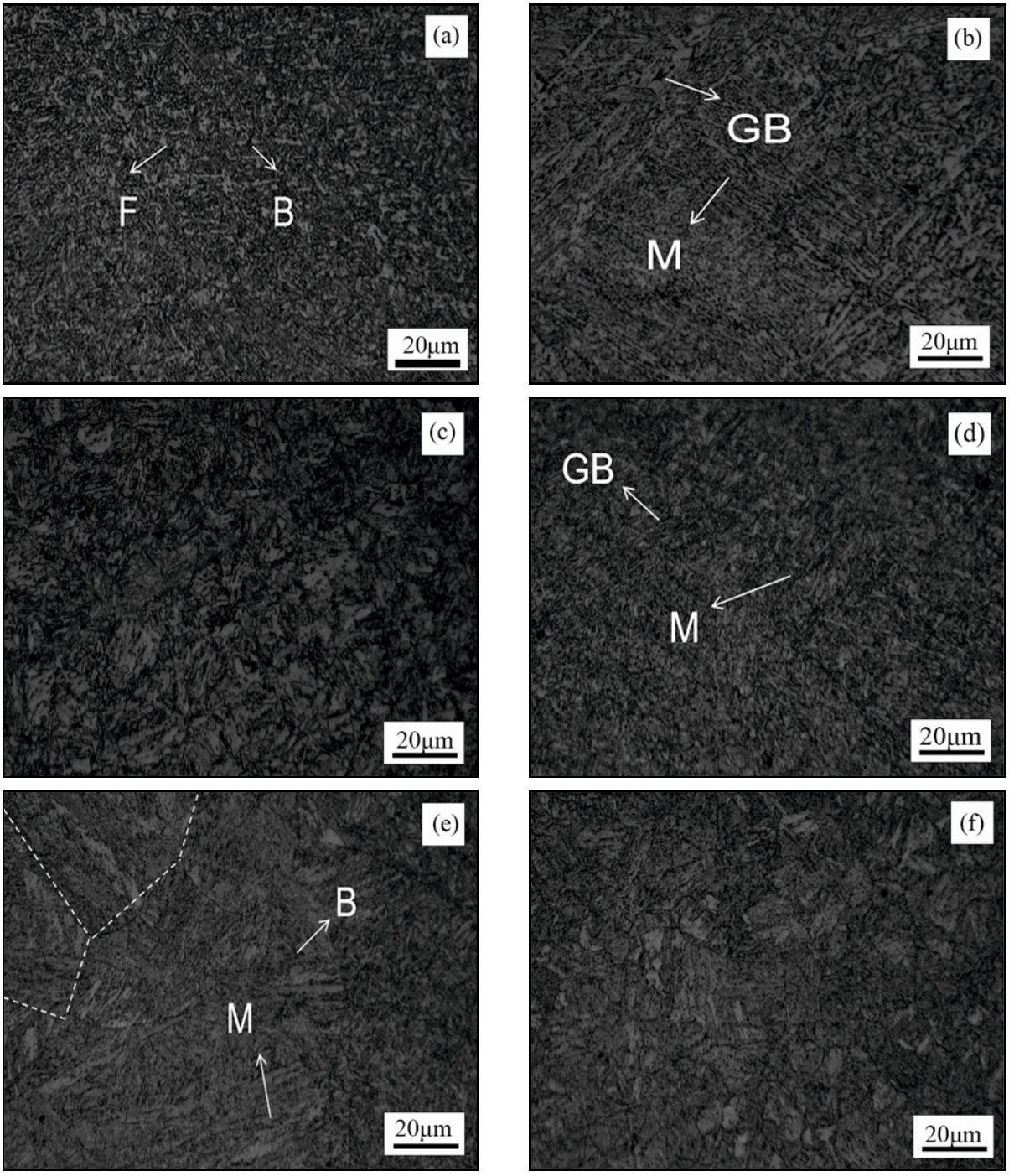

Fig. 3a–f. Microstructure organization of various regions of welded joints under different welding processes: Inter-pass temperature 150 °C, 60 °V-bevel: (a) WM, (b) CGHAZ, and (c) FGHAZ; Inter-pass temperature 30 °C, 60 °V-bevel: (d) WM, (e) CGHAZ, and (f) FGHAZ; Inter-pass temperature 30 °C.

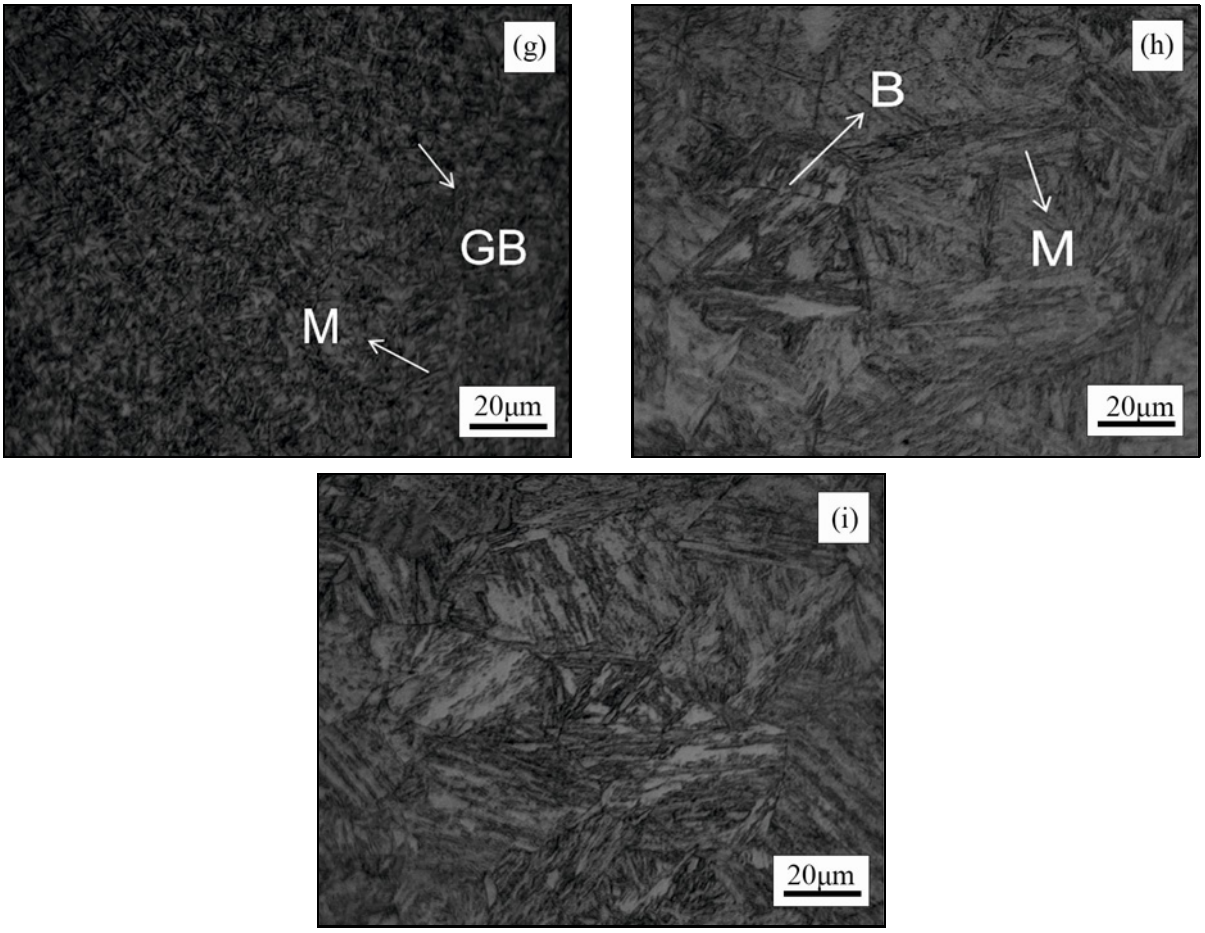

Fig. 3g–i. Microstructure organization of various regions of welded joints under different welding processes: Inter-pass temperature 30 °C, 40 °V-bevel: (g) WM, (h) CGHAZ, and (i) FGHAZ.

testing machine measured the three-point bending and tensile test. The surface microhardness test was carried out by the KB30S-FA automatic Vickers hardness testing machine (test load of 100 g, loading time of 10 s). SANS metal pendulum impact tester was used for the impact test (–40 °C), and the impact absorption energy was averaged.

3. Results and discussion

3.1. Macro-metallography and microstructure

The metallography of three different welded joints is shown in Fig. 2. The welds are well formed, showing a smooth and complete outline, and no welding defects such as unfused, impermeable cracks and porosity were found.

The welded joint was composed of three different zones: weld zone (WZ), heat-affected zone (HAZ), and base material (BM) [25]. The performance of the welded joints can be effectively improved by preheating before welding and then cooling to room temperature. The inter-pass temperature affects the cooling rate, thereby affecting the welding thermal cycle process, affecting the microstructure and properties of welded joints [26]. The HAZ next to the weld is the weakest region of the welded joint because of its poor plasticity and toughness [27]. The grains of the HAZ in the welded joint grow seriously during the welding thermal cycle process, which in turn affects the mechanical properties and welding performance. Therefore, the changes in the weld microstructure, coarse-grained and fine-grained zones, were studied at different inter-pass temperatures.

The microstructure zone of various regions of the welded joints under different welding processes is shown in Fig. 3. Figure 3a shows the weld (WM) organization of the layer temperature of 150 °C and 60 °V, which is mainly composed of ferrite (ferrite, F) and granular bainite (GB); Fig. 3b is the coarse-grained heat-affected zone (CGHAZ), with the main organization of lath martensite (martensite, M) and bainite; Fig. 3c is the fine-grained heat-affected zone (FGHAZ) organization, which is mainly massive ferrite, and the intracrystalline consists of granular bainite; Fig. 3d is the WM at layer temperature of 30 °C and 60 °V, mainly M + GB; Fig. 3e is the CGHAZ organization

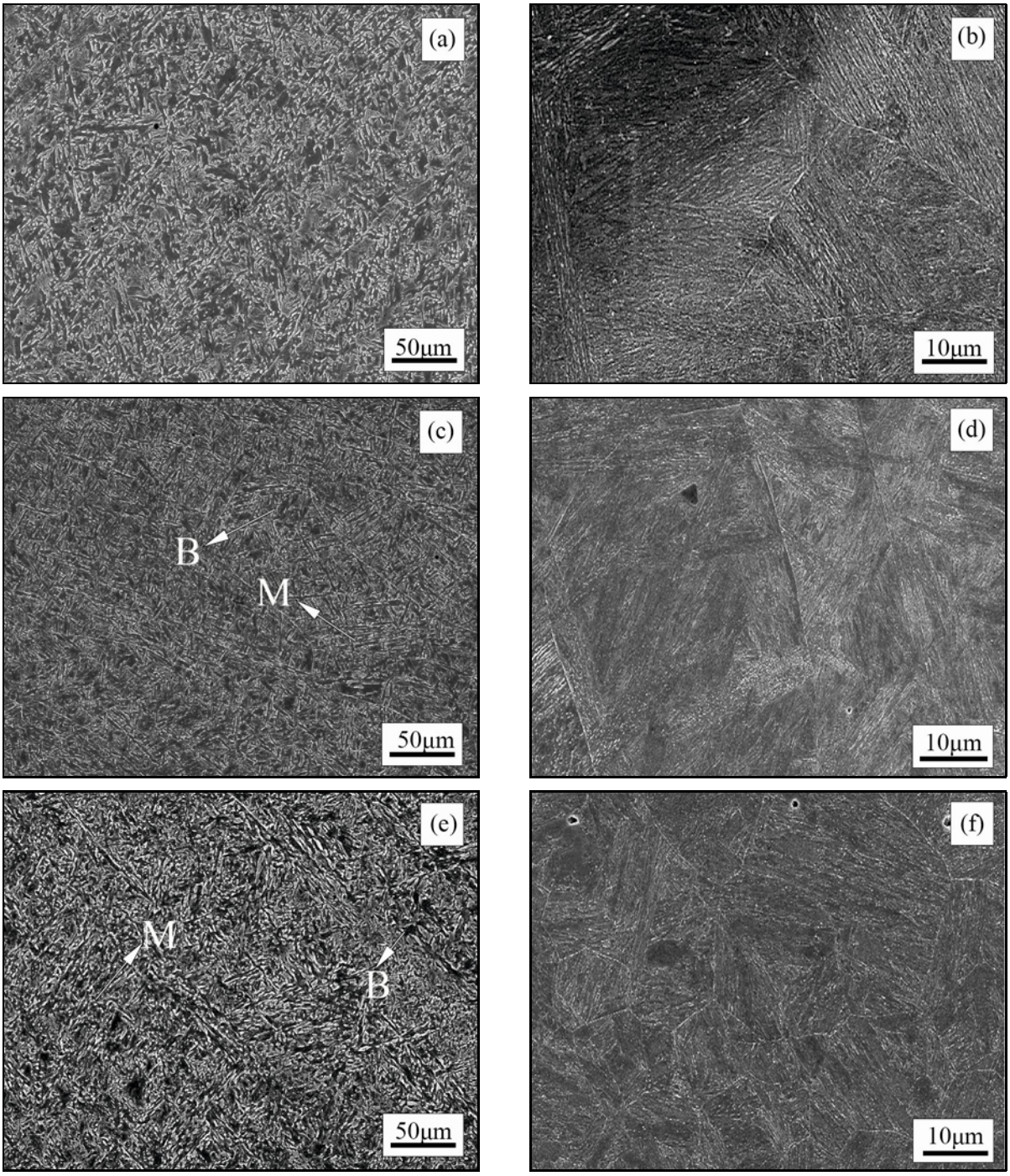

Fig. 4. Metallographic microstructure of welded joints with different welding process parameters: Inter-pass temperature 150 °C, 60 °V-bevel: (a) WM and (b) CGHAZ; Inter-pass temperature 30 °C, 60 °V-bevel: (c) WM and (d) CGHAZ; Inter-pass temperature 30 °C, 40 °V-bevel: (e) WM and (f) CGHAZ.

at layer temperature of 30 °C and 60 °V, which consists mainly of M + GB; and Fig. 3f is the FGHAZ organization, which is mainly M, with granular bainite distributed in the slats; Fig. 3g shows the WM with layer temperature 30 °C and 40 °V, mainly composed of M + GB; Fig. 3h shows the CGHAZ organization, mainly composed of M; and Fig. 3i shows the FGHAZ organization, mainly M.

When the inter-pass temperature cools from 150 to 30 °C, the cooling rate increases and the microstructure changes from F + GB to M + GB. The main reason for the change in the microstructure of welded joints is that the joints are cooled from a temperature above AC3 to different inter-pass temperatures, and the cooling rate is not the same. The cooling rate accelerates as the inter-pass temperature decreases from

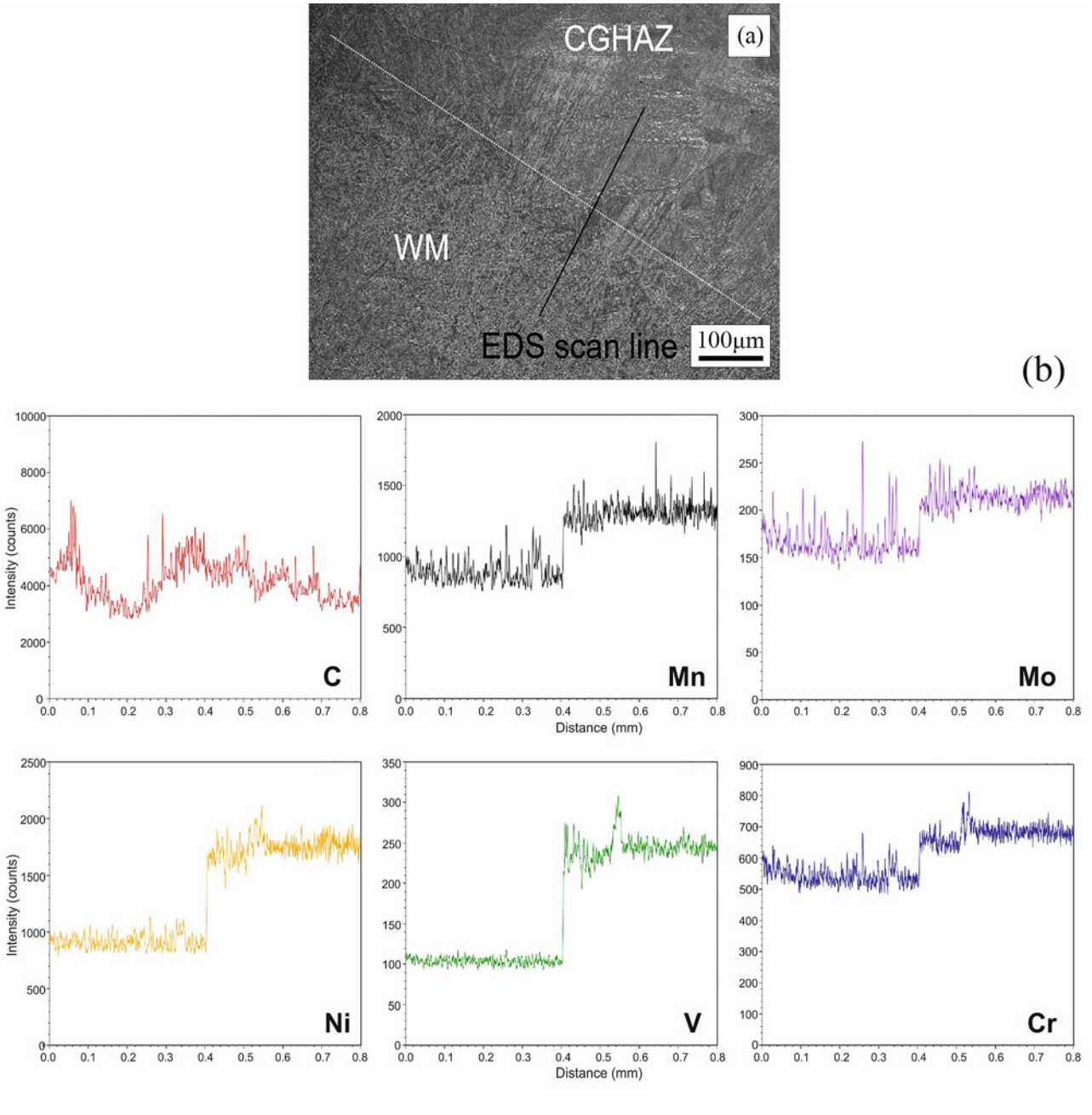

Fig. 5a,b. Line scan analysis with different welding parameters: Inter-pass temperature 150 °C, 60 °V-bevel: (a) EDS Scanning position and (b) EDS test results; Inter-pass temperature 30 °C.

150 to 30 °C. During the phase transformation process, low-temperature transformation of high-strength steel will occur. This can produce a low-temperature martensite microstructure, and the weld microstructure appears in the lath martensite, with a middle distribution of GB organization. With the interlayer temperature cooling to room temperature, the CGHAZ microstructure is still dominated by low carbon martensite with high microhardness, but the number of GBs in the CGHAZ microstructure decreases. The degree of coarsening becomes smaller, and the primary austenite grain boundaries can be seen. The inter-pass temperature dropped from 150 to 30 °C, and the FGHAZ microstructure changed from ferrite and granular bainite to low-carbon martensite.

With the change of bevel form from 60 °V to 40 °V, the WM is still a mixed microstructure of M + GB, and the microstructure change is not obvious. As shown in Fig. 3e, lath martensite is organized in the CGHAZ, and there is a certain amount of granular bainite. As the bevel angle becomes smaller, the CGHAZ grain coarsening tends to be smaller than the 60 °V-

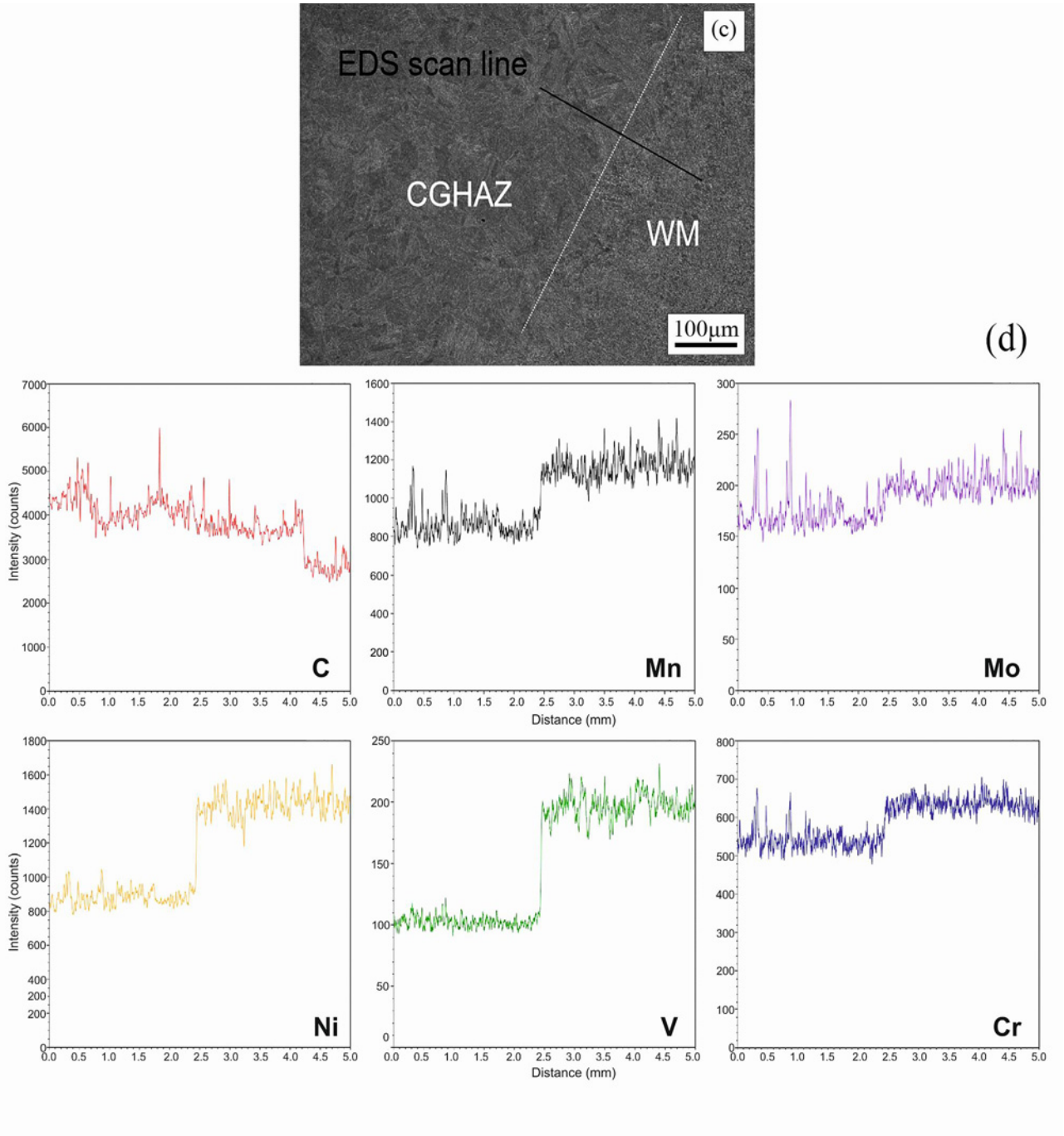

Fig. 5c,d. Line scan analysis with different welding parameters: Inter-pass temperature 30 °C, 60 °V-bevel: (c) EDS Scanning position and (d) EDS test results; Inter-pass temperature 30 °C.

-type sample, with a certain amount of site-direction relationship, and the amount of granular bainite is reduced. As the bevel angle becomes smaller, the FG-HAZ zone is still low carbon martensite + granular bainite, but the amount of granular bainite is reduced, and the degree of coarsening of the zone becomes smaller. The original austenite grain boundaries can be seen.

The change of microstructure with the inter-pass temperature and bevel form was observed by SEM (Fig. 4). With the decrease of inter-pass temperature, the weld zone changes from ferrite and granular bainite to slab martensite and bainite. The coarsening trend of lath martensite decreased, and the grain boundaries of proto-austenite decreased in the microstructure of HAZ. From 60 °V-type to 40 °V-type, the weld microstructure is still lath martensite + lower bainite, and the lath martensite coarsening degree is the smallest in HAZ, and the original austenite grain boundary can be seen.

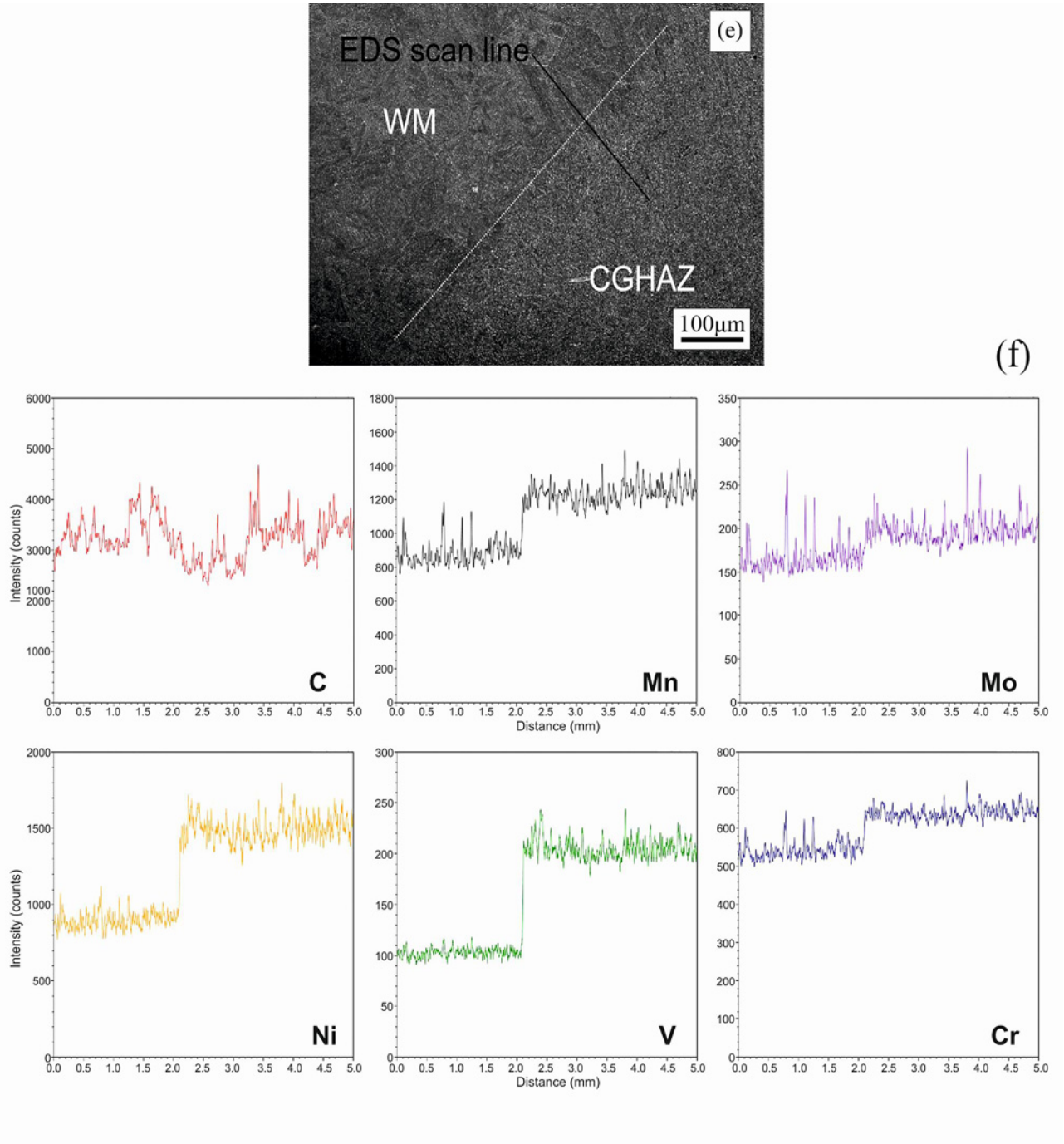

Fig. 5e,f. Line scan analysis with different welding parameters: Inter-pass temperature 30 °C, 40 °V-bevel: (e) EDS Scanning position and (f) EDS test results.

The welded joints were analyzed by EDS line scanning, and the positions of the line scanning are shown in Figs. 5a,c,e. The EDS test results are shown in Figs. 5b,d,f. The decrease in inter-pass temperature shows no obvious change in C, Cr, and Mo elements. The content of Ni, V, and Mn elements decreases, among which, the content of the V element in the welding wire is about 10 times that of the base metal, thus leading to the obvious difference in changes in the weld seam and the heat-affected zone. The amount of Mn, Ni, and V elements in the welding wire is significantly higher than that in the base metal, and the elements of the welded joint can be well transitioned. With the change of the bevel angle, there is no significant change in the other elements, except for a decrease in C elements. Mn element has the effect of solid solution strengthening and stabilizing austenite, which can increase the hardenability of steel, and the

Table 5. Tensile and bending properties of welded joints

Inter-pass temperature (℃)	Beveling form	Tensile strength (MPa)	Fracture position	Bending result
150	60°V	1080	HAZ	eligible
30	60°V	1111	HAZ	eligible
30	40°V	1135	HAZ	eligible

Table 6. Impact performance of welded joints (–40 ℃)

Sample number	Fracture position (mm)	Shock absorption (J)			Average (J)
1	WM	29	36	27	30
	FL	28	27	30	28
	FL + 2	38	40	36	38
2	WM	30	28	32	30
	FL	28	29	30	29
	FL + 2	40	51	55	49
3	WM	29	32	30	30
	FL	33	34	28	32
	FL + 2	60	81	87	79

low content of Mn leads to insufficient strength and hardness of high-strength steel [28]. Cr element has the role of the second phase strengthening, enhancing the tensile strength of the welded joints of steel [29]. Adding elements of V can inhibit grain growth, thus improving the mechanical properties of steel.

3.2. Mechanical properties

The tensile and flexure tests are carried out at room temperature, with two specimens in each group, and the average value is taken as the final result. Table 5 shows the tensile and flexure test results of 1100 MPa grade high-strength steel welded joints. The guided bending method was adopted for the flexure test. As shown in Table 4, the results of the three bending specimens are qualified. From the data, all three kinds of fractures are in HAZ, mainly because there are many martensite and granular bainite microstructures in HAZ. The slat martensite microhardness is relatively high, the plasticity and toughness are relatively poor, and a large number of granular bainite will produce a stress concentration, which becomes a potential source of cracking, making the heat-affected zone a weak region. As the inter-pass temperature decreases, the tensile strength increases. The tensile strength is further increased with the decrease in the bevel angle. This is because selecting a reasonable welding process during welding will avoid the formation of coarse grains, coarsening of the zone in the heat-affected zone of welding, and the poor performance of the granular bainite region.

Table 6 shows the results of V-impact testing of welded joints under different welding processes, and impact test at –40 ℃ on the weld, bone line, and bone line + 2 position. The average absorbed energy of the impact is higher than 27 J. The trend of energy impact is that the heat-affected zone is greater than that of the weld, and the energy impact of the fusion line is the smallest. The impact toughness of the welded joints under the inter-pass temperature 30 ℃, 40 °V--bevel is the highest, as shown in Fig. 6. Mainly because the low-carbon martensite zone is fine and uniform, and the number of granular bainite decreases sharply, so the impact toughness of the heat-affected

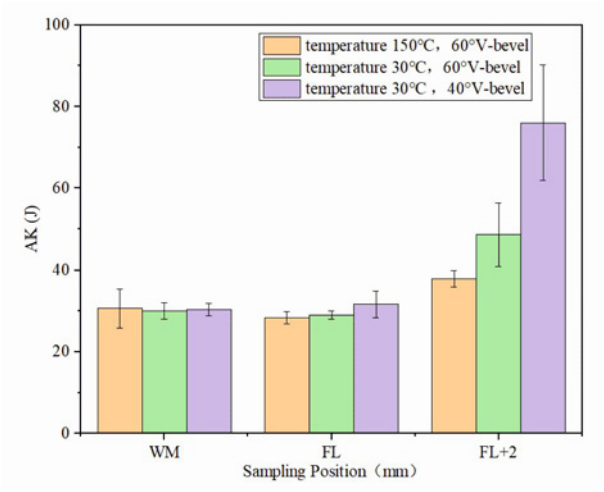

Fig. 6. Change of impact work with different welding process parameters.

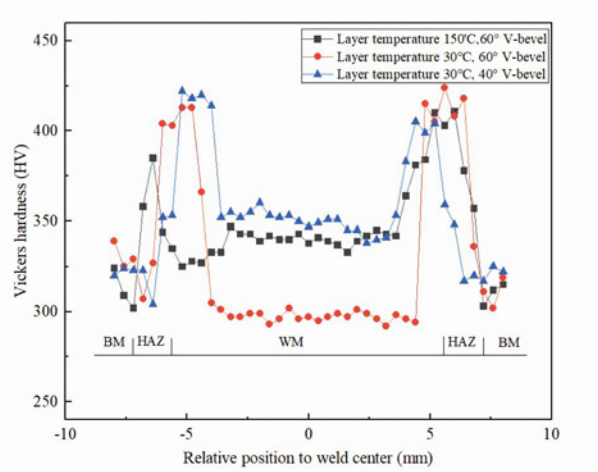

Fig. 7. Distribution curve of microhardness of welded joints under different welding processes.

zone is relatively high, in the same bevel form. Under the same bevel form, with the decrease of inter-pass temperature and the acceleration of cooling rate, slat martensite appears in the weld microstructure, which has a certain toughness and relatively high impact energy. At the same inter-pass temperature, the zone becomes fine and uniform with the decrease of the bevel angle, and the number of granular bainite decreases. The number of granular bainite is reduced, and the impact toughness becomes more excellent.

The microhardness test was conducted on specimens with different inter-pass temperatures and bevel forms. The test location was about 2 mm below the rear welding surface with less impact [30], and the load was 9.8 N. The results of the test are shown in Fig. 7. The hardness value of the base metal is stable, about 310 HV, and the microhardness distribution trend of the welded joints with different processes is roughly the same, with the weld's hardness value being higher than that of the base metal. The center extends to the base metal, and the maximum microhardness is obtained in the fine-grain region. A comparison of three different processes found that with the inter-pass temperature of 150 ℃, the bevel form of 60 °V-type weld zone microhardness value is the lowest, about 340 HV, and the heat affected zone has the lowest hardness value of the grain coarse crystal zone, about 380 HV. When the inter-pass temperature is 30 ℃ and the bevel form is 60 °V-type, the weld zone microhardness value is higher, about 345 HV, heat-affected zone has the high hardness value of the coarse crystal zone, about 410 HV; with the layer temperature of 30 ℃, the bevel form of 60 °V-type weld zone hardness value is about 410 HV; with the layer temperature of 30 ℃, the bevel form of 40 °V-type weld zone hardness value is the highest, about 351 HV, and the heat-affected zone of coarse crystal area hardness value is the highest, about 413 HV. Due to the coarse-grained area near the base material, the grain grows seriously, resulting in lath martensite and granular bainite. The coarse--grain area has the maximum microhardness value due to the microstructure and fine-grain strengthening of lath martensite.

3.3. *Fracture morphology*

The fracture morphology of the heat-affected zone under three different welding processes is shown in Fig. 8. The fracture morphology of the 150 ℃, 60 °V--bevel sample is characterized by quasi-cleavage fracture. The radiating area of the fracture displays obvious cleavage facets, and the morphology features are cleavage steps and river patterns. The fiber region of the fracture is a small dimple with inclusion particles, and the grain boundary of the HAZ is thick, which lowers the impact toughness of the other two samples. The fracture morphology of 30 ℃, 60 °V-bevel samples is also quasi-cleavage fracture, which is composed of cleavage step + river pattern, and the fracture fiber region is composed of dense and deep dimples. The radiating zone of the 30 and 40 °V-bevel samples is characterized by quasi-cleavage fracture, which is composed of cleavage steps and river patterns. The fiber region of the fracture is dense and small, and cleavage facets form a tear edge. Therefore, it has a higher fracture toughness and higher impact energy.

4. Conclusions

1. In this paper, flux-cored wire CO_2 gas shielded welding of Q1100E high-strength steel was carried out for different inter-pass temperatures and bevel forms. All of them resulted in welded joints that were free of defects and well-formed.

2. The results show that the microstructure of welding metal transforms from ferrite and granular bainite to lath martensite and granular bainite as the inter-pass temperature decreases. The coarsening trend of the lath martensite becomes smaller, and the number of granular bainite is relatively small. With the decrease of the bevel angle, the weld microstructure is still lath martensite + granular bainite. The lath martensite coarsening degree decreases, and the number of granular bainite becomes less.

3. When the bevel was 60 °V-shaped, the tensile strength of the joints increased from 1080 to 1111 MPa, and the impact toughness of HAZ increased from 38 to 49 J with the decrease of inter-pass temperature. When the inter-pass temperature was 30 ℃, the tensile strength of the joint increased from 1111 to 1135 MPa, and the impact toughness of the HAZ increased from 49 to 79 J with the decrease of the bevel angle. When the inter-pass temperature was 30 ℃ and

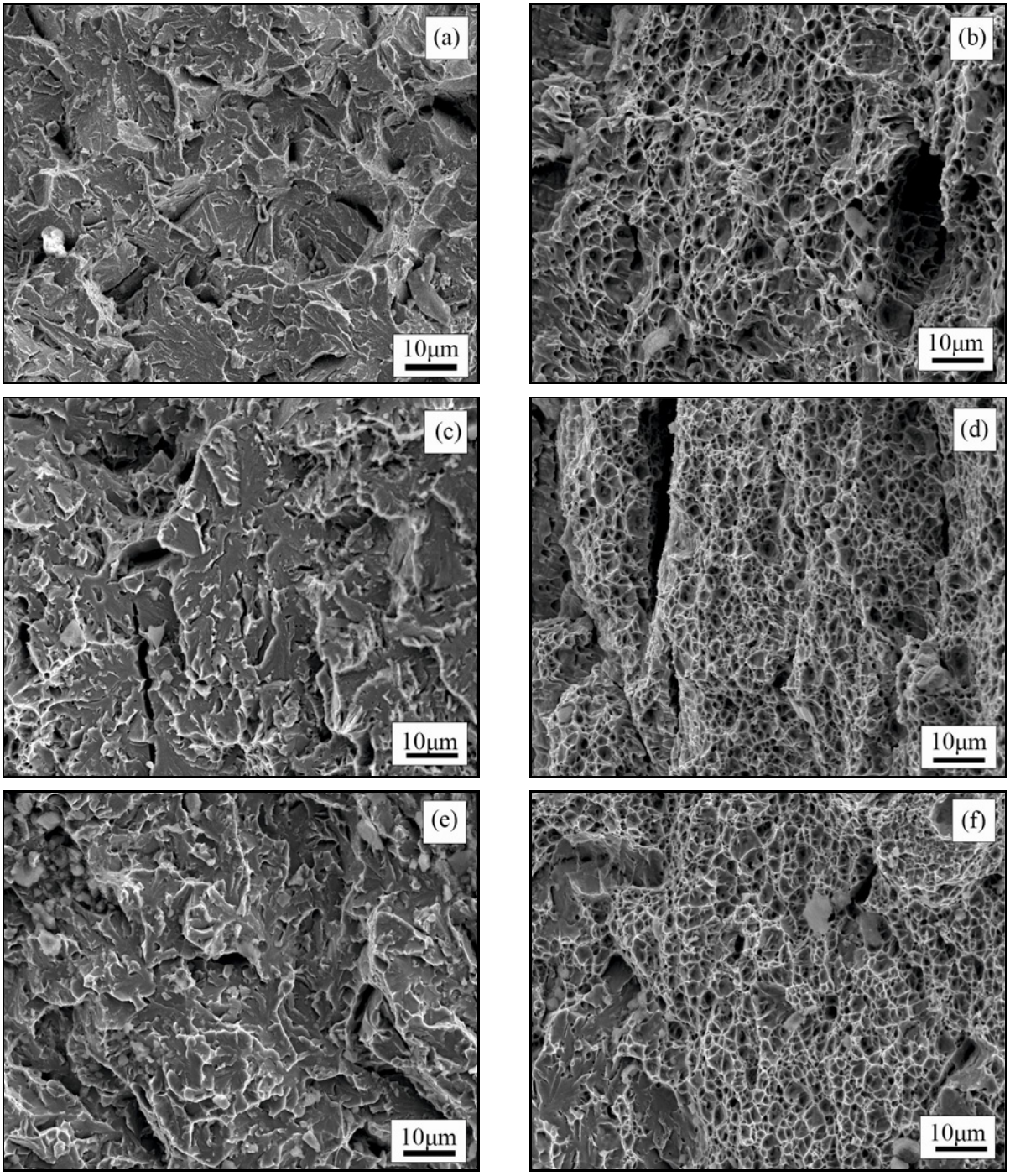

Fig. 8. Impact fracture morphology for different welding processes: Layer temperature 150 °C, 60 °V-bevel: (a) radiation zone and (b) fibrous zone; Layer temperature 30 °C, 60 °V-bevel: (c) radiation zone and (d) fibrous zone; Layer temperature 30 °C, 40 °V-bevel: (e) radiation zone and (f) fibrous zone.

the bevel was 40 °V-shaped, the maximum microhardness was obtained in the coarse-grained region, reaching 413 HV.

Acknowledgement

No public, commercial or non-profit organization funded this study.

References

[1] K. Yang, F. Wang, D. Duan, T. Zhang, Ch. Luo, Y. Cressault, Z. Yu, L. Yang, H. Li, Experimental investigation of integrated circular triple-wire pulse GMAW of Q960E high-strength steel for construction machinery, Journal of Materials 14 (2021) 375. https://doi.org/10.3390/ma14020375

[2] X. Meng, G. Qin, Y. Zhang, B. Fu, Z. Zou, High speed TIG-MAG hybrid arc welding of mild steel plate, Journal of Materials Processing Techn. 214 (2014) 2417–2424. https://doi.org/10.1016/j.jmatprotec.2014.05.020
[3] M. Zhou, Effect of laser-MIG hybrid welding on microstructure and properties of seismic steel plate for buildings, Results in Physics 12 (2019) 840–845. https://doi.org/10.1016/j.rinp.2018.12.054
[4] A. Su, H. Yang, Y. Wang, O. Zhao, Experimental and numerical investigations of S960 ultra-high strength steel welded I-section beams with in-plane flexural failure, Thin-Walled Structures 190 (2023) 110969. https://doi.org/10.1016/J.TWS.2023.110969
[5] X. Tian, L. Chao, Variation of plate shape in laminar cooling process of low carbon bainitic steel Q690D, Journal of Materials Engineering and Performance 32 (2023) 10669–10679. https://doi.org/10.1007/s11665-023-07885-7
[6] H. Guo, X. Guan, Y. Pan, D. Yang, Y. Zhao, Experimental research on fatigue crack growth behavior of Q690D high strength steel, Journal of Constructional Steel Research 220 (2024) 108809. https://doi.org/10.1016/j.jcsr.2024.108809
[7] Y. Li, T. Long, Z. Luo, C. Wen, Z. Zou, L. Jin, B. Li, Numerical and experimental investigations on dynamic behaviors of a bolted joint rotor system with pedestal looseness, Journal of Sound and Vibration 571 (2024) 118036. https://doi.org/10.1016/j.jsv.2023.118036
[8] Y. Li, Z. Zhu, Ch. Wen, K. Liu, Z. Luo, L. Long, Rub-impact dynamic analysis of a dual-rotor system with bolted joint structure: Theoretical and experimental investigations, Mechanical Systems & Signal Processing 209 (2024) 111144. https://doi.org/10.1016/j.ymssp.2024.111144
[9] D. Li, Z. Huang, B. Uy, H. T. Thai, C. Hou, Slenderness limits for fabricated S960 ultra-high-strength steel and composite columns, Journal of Constructional Steel Research 159 (2019) 109–121. https://doi.org/10.1016/j.jcsr.2019.04.025
[10] H. Ban, G. Shi, A review of research on high-strength steel structures, Proceedings of the Institution of Civil Engineers 171 (2018) 625–641. https://doi.org/10.1680/jstbu.16.00197
[11] F. Lei, G. Xu, Y. Yong, J. Yang, X. Jian, The application and research progress of high strength and high performance steel in building structure, IOP Conference Series Materials Science and Engineering 392 (2018) 022008. https://doi.org/10.1088/1757-899X/392/2/022008
[12] L. Yang, F. Yin, J. Wang, A. Bilal, A. H. Ahmed, M. Lin, Local buckling resistances of cold-formed high-strength steel SHS and RHS with varying corner radius, Thin-Walled Structures 172 (2022) 108909. https://doi.org/10.1016/j.tws.2022.108909
[13] A. Su, Y. Sun, Y. Liang, O. Zhao, Membrane residual stresses and local buckling of S960 ultra-high strength steel welded I-section stub columns, Thin-Walled Structures 161 (2021) 107497. https://doi.org/10.1016/j.tws.2021.107497
[14] X. Yang, X. Di, X. Liu, D. Wang, C. Li, Effects of heat input on microstructure and fracture toughness of simulated coarse-grained heat affected zone for HSLA steels, Materials Characterization 155 (2019) 109818. https://doi.org/10.1016/j.matchar.2019.109818
[15] H. Ban, G. Shi, Overall buckling behaviour and design of high-strength steel welded section columns, Journal of Constructional Steel Research 143 (2018) 180–195. https://doi.org/10.1016/j.jcsr.2017.12.026
[16] A. Su, Y. Liang, Q. Zao, Experimental and numerical studies of S960 ultra-high strength steel welded I-section columns, Thin-Walled Structures 159 (2021) 107166. https://doi.org/10.1016/j.tws.2020.107166
[17] B. Huang, W. F. Zhang, Local-overall interactive buckling of high-strength steel welded I-section columns under axial compression, Thin-Walled Structures 157 (2020) 106964. https://doi.org/10.1016/j.tws.2020.106964
[18] S. Chen, H. Fang, J. Liu, T. M. Chan, Design for local buckling behaviour of welded high-strength steel I-sections under bending, Thin-Walled Struct. 172 (2022) 108792. https://doi.org/10.1016/j.tws.2021.108792
[19] L. Lan, X. Kong, Ch. Qiu, D. Zhao, Influence of microstructural aspects on impact toughness of multi-pass submerged arc welded HSLA steel joints, Materials & Design 90 (2016) 488–498. https://doi.org/10.1016/j.matdes.2015.10.158
[20] S. R. Nathan, V. Balasubramanian, S. Malarvizhi, A. G. Rao, Effect of welding processes on mechanical and microstructural characteristics of high strength low alloy naval grade steel joints, Defence Technology 11 (2015) 308–317. https://doi.org/10.1016/j.dt.2015.06.001
[21] C. Sun, P. X. Fu, X. P. Ma, H. H. Liu, D. Z. Li, Effect of matrix carbon content and lath martensite microstructures on the tempered precipitates and impact toughness of a medium-carbon low-alloy steel, Journal of Materials Research and Technology 9 (2020) 7701–7710. https://doi.org/10.1016/j.jmrt.2020.05.002
[22] P. Haslberger, S. Holly, W. Ernst, R. Schnitzer, Microstructure and mechanical properties of high-strength steel welding consumables with a minimum yield strength of 1100 MPa, Journal of Materials Science 53 (2018) 696–6979. https://doi.org/10.1007/s10853-018-2042-9
[23] C. Dong, A. M. Zhao, X. T. Wang, Q. H. Pang, H. B. Wu, Microstructure and properties of 1100 MPa grade low-carbon hot-rolled steel by laser welding, Journal of Iron and Steel Research International 25 (2018) 228–234. https://doi.org/10.1007/s42243-018-0025-3
[24] Z. J. Liu, C. A. Wang, Y. H. Su, F. D. Zhao, L. C. Li, Effect of heat input on structure and mechanical properties of low matched welded joint in a 1000 MPa grade steel, Advanced Materials Research 418–420 (2012) 1184–1187. https://doi.org/10.4028/www.scientific.net/AMR.418-420.1184
[25] X. Yun, Y. Zhu, X. Meng, L. Gardner, Welded steel I-section columns: Residual stresses, testing, simulation and design, Engineering Structures 282 (2023) 115631. https://doi.org/10.1016/j.engstruct.2023.115631
[26] L. Gerard, L. Li, M. Kettler, N. Boissonnade, Recommendations on the geometrical imperfections definition for the resistance of I-sections, Journal of Constructional Steel Research 162 (2019) 105716. https://doi.org/10.1016/j.jcsr.2019.105716
[27] Y. Jing, K. Jiang, O. Zhao, L. Gardner, Web crippling of stainless steel built-up I-sections under End-Two-

-Flange loading: Tests, simulations and design, Engineering Structures 304 (2024) 117576. https://doi.org/10.1016/j.engstruct.2024.117576

[28] J. Wang, S. Afshan, M. Gkantou, M. Theofanous, C. Baniotopoulos, L. Gardner, Flexural behaviour of hot-finished high strength steel square and rectangular hollow sections, Journal of Constructional Steel Research 121 (2016) 97–109. https://doi.org/10.1016/j.jcsr.2016.01.017

[29] S. Gao, N. Li, Y. Huang, J. Yan, L. Yang, Experimental study of fatigue behaviour of Q690qENH bridge weathering high-strength steel welded joints, Thin-Walled Structures 190 (2023) 110954. https://doi.org/10.1016/j.tws.2023.110954

[30] H. Qi, Q. Pang, W. Li, S. Bian, The influence of the second phase on the microstructure evolution of the welding heat-affected zone of Q690 steel with high heat input, Materials (2024) 1996–1944. https://doi.org/10.3390/ma17030613